Biosensors and Bioelectronics 140 (2019) 111353

Contents lists available at ScienceDirect

Biosensors and Bioelectronics

journal homepage: www.elsevier.com/locate/bios

Ultrasensitive analysis of carcinoembryonic antigen based on MoS_2-based electrochemical immunosensor with triple signal amplification

Shao Su[a], Qian Sun[a], Ling Wan[a], Xiaodan Gu[a], Dan Zhu[a], Yi Zhou[b], Jie Chao[a,**], Lianhui Wang[a,*]

[a] Key Laboratory for Organic Electronics and Information Displays (KLOEID), Jiangsu Key Laboratory for Biosensors, Institute of Advanced Materials (IAM), National Synergetic Innovation Center for Advanced Materials (SICAM), Nanjing University of Posts and Telecommunications, 9 Wenyuan Road, Nanjing, 210023, China
[b] College of Basic Medicine, Chengdu University of Traditional Chinese Medicine, Chengdu, 611137, China

ARTICLE INFO

Keywords:
Immunosensor
Signal amplification
Nanoprobe
Catalytic reaction

ABSTRACT

Ultrasensitive detection of cancer biomarkers has shown great promise for precision medicine. Here, a triple signal amplification strategy was developed for analysis of carcinoembryonic antigen (CEA) by using MoS_2-based nanocomposites. Gold nanoparticles-decorated molybdenum disulfide nanocomposite (MoS_2-AuNPs) was used to construct the modified electrode and nanoprobe, which could efficiently amplify electrochemical signal due to its large surface area and high catalytic ability. Horseradish peroxidase (HRP)-labelled carcinoembryonic monoclonal antibody (anti-CEA) and HRP were used to co-construct the MoS_2-based nanoprobe, which could further amplify the electrochemical signal by catalyzing o-phenylenediamine (o-PD) in the presence of hydrogen peroxide (H_2O_2). Expectedly, an excellent analytical performance for CEA detection was obtained, such as wide detection range (10 fg mL^{-1}-1 ng mL^{-1}), ultralow detection limit (1.2 fg mL^{-1}), high selectivity and good stability, suggesting this immunosensor could detect CEA in real samples.

1. Introduction

Accurate, sensitive, fast biomarkers detection shows a great role in promising disease analysis (Yang et al., 2011; Chen et al., 2011; Yang et al., 2011). Due to ultralow concentration of biomarkers (such as microRNA and antigens), development of high-performance strategies for biomarkers detection has attracted more and more researchers' attention (Miao et al., 2017; Wen et al., 2013; Yan et al., 2008). As we know, electrochemical immunosensor is considered as a powerful tool to detect biological molecules due to its highly specific recognition ability and high sensitivity (Fan et al., 2000; Ge et al., 2011; Wan et al., 2011, 2013). To meet the needs of practical application, sandwich-type immunosensors with signal amplification units have been extensively developed to improve the sensitivity (Tang et al., 2008; Li et al., 2018; Shen et al., 2015; Wu et al., 2015; Zhou et al., 2013). On the basis of this concept, several amplification strategies have been designed to efficiently enhance the detection performance, including nanomaterials-based probes (Kong et al., 2011; Ren et al., 2017; Yang et al., 2017; Zhou et al., 2015), nanomaterials-based catalytic effect (Huang et al., 2018; Li et al., 2015; Sun et al., 2014; Zhao et al., 2014) and enzyme-assisted amplification (Li et al., 2015; Lin et al., 2015; Sun et al., 2013; Wang et al., 2017; Yuan et al., 2012). For example, Yuan and co-worker used graphene nanocomposites functionalized with Au@Pd core/shell bimetallic to load numbers of thionine, horseradish peroxidase and secondary antibodies (Ab2). The formation of signal enhancers greatly improved detection performance by utilizing catalytic reaction, which could detect down to 0.006 U mL^{-1} carbohydrate antigen 19–9 (CA19-9) (Yang et al., 2015a). Although great advances of electrochemical immunosensors have been achieved, it is still a challenge to explore high-performance immunosensors for ultrasensitive detection of biomarkers with multiple signal amplification (Farka et al., 2017; Pei et al., 2012).

Nanomaterials, including noble metal nanostructures (Wang et al., 2014; Liu et al., 2012), layered nanomaterials (Du et al., 2010; He et al., 2010; Jiang et al., 2015; Lin et al., 2012), carbon nanotubes (Lu et al., 2012; Zuo et al., 2009) and metal oxides (Feng et al., 2016), have been extensively introduced into the construction of modified electrodes or nanoprobes due to their excellent properties, which could greatly improve the sensitivity of electrochemical immunosensors. To further enhance the detection performance, introduction of enzyme amplification has become an efficient strategy (Li et al., 2008; Peng et al., 2018; Yang et al., 2015b, 2016). For instance, Zhong et al. immobilized horseradish peroxidase (HRP)-conjugated carcinoembryonic monoclonal antibody (anti-CEA) on nanogold-enwrapped graphene

* Corresponding author.
** Corresponding author.
E-mail addresses: iamjchao@njupt.edu.cn (J. Chao), iamlhwang@njupt.edu.cn (L. Wang).

https://doi.org/10.1016/j.bios.2019.111353
Received 2 April 2019; Received in revised form 18 May 2019; Accepted 24 May 2019
Available online 25 May 2019
0956-5663/

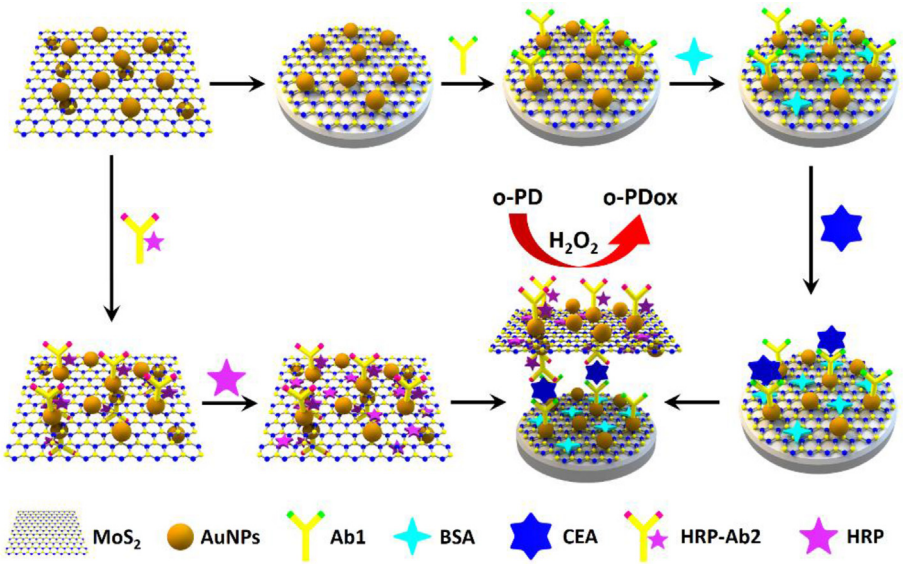

Scheme 1. Scheme of MoS_2-based immunosensor for CEA analysis.

nanocomposites surface as a signal enhancer to improve the detection performance (Zhong et al., 2010). Zhou's group used HRP to block the graphene-based nanoprobe. With the catalytic effect of HRP, the proposed electrochemical immunosensor could detect 50 pg mL^{-1} immunoglobulin G (IgG) (Yang et al., 2011).

Gold nanoparticles-decorated MoS_2 nanocomposite (MoS_2-AuNPs) had been extensively used as an electrode modified material to construct electrochemical immunosensors due to its excellent conductivity and large surface area (Su et al., 2015; Devi et al., 2019; Pang et al., 2018; Peng et al., 2018). However, most of works only used MoS_2-AuNPs nanocomposite as an electrode modified material. It should be noted that MoS_2-AuNPs nanocomposite was also an ideal nanomaterial to construct nanoprobes for the preparation of electrochemical sensors (Su et al., 2017). Inspired by the above works, we constructed an enzyme-assisted signal amplification strategy for CEA analysis by utilizing the advantages of MoS_2-AuNPs nanocomposites and the catalytic effect of biological enzymes. As shown in Scheme 1, a large number of anti-CEA (Ab1) were immobilized on MoS_2-AuNPs film modified electrode surface to efficiently capture target CEA. Meanwhile, HRP-anti-CEA (Ab2) and HRP were co-functionalized on MoS_2-AuNPs surface to form MoS_2-based nanoprobes, which could obviously amplify electrochemical signal. It should be noted that such efficient amplification in electrochemical signal was ascribed to the designed triple amplification strategy. First, MoS_2-AuNPs nanocomposites had been proved to be efficient enzyme mimics and excellent conductivity, which could facilitate the reaction between o-PD and H_2O_2 (Xiu et al., 2015). Second, MoS_2-AuNPs nanocomposites possessed large surface area, which could load large amounts of anti-CEA and HRP-anti-CEA. The HRP labelled on the anti-CEA could catalyze o-PD in the presence of H_2O_2, further amplifying the detection signal. Third, the introduction of HRP blocked the nonspecific adsorption of immunosensor, which could triply amplify the electrochemical signal due to the enzymatically catalytic reaction. As a result, the designed immunosensor exhibited high sensitivity and selectivity for CEA detection in ideal buffer and real samples.

2. Experimental section

2.1. Reagents and apparatus

All the reagents, chemicals and characterized apparatus were listed in Supporting Information.

2.2. Synthesis of MoS_2-AuNPs-based nanoprobes

Synthesis of MoS_2 nanosheets and MoS_2-AuNPs nanocomposites were recorded in the Supporting Information (Su et al., 2014, 2016, 2019).

The MoS_2-AuNPs nanocomposites (1.0 mg mL^{-1}) were incubated with 1.0 mg mL^{-1} HRP-anti-CEA solution at 4 °C for 12 h. After that, the unbound HRP-anti-CEA was removed by 0.1 M phosphate buffer (PB). Then, the purified HRP-anti-CEA/MoS_2-AuNPs nanoprobe was blocked by HRP to avoid the nonspecific absorption and amplify the electrochemical signal. Finally, the purified product was defined as HRP/HRP-anti-CEA/MoS_2-AuNPs nanoprobe, which was re-dispersed and stored at 4 °C. Similarly, BSA/HRP-anti-CEA/MoS_2-AuNPs and HRP-anti-CEA/AuNPs nanoprobes were prepared by using the similar procedure.

2.3. Preparation of MoS_2-based detection strategy

5 μL MoS_2-AuNPs nanocomposite solution was modified onto the cleaned glassy carbon electrode (GCE). Then, 100 μg mL^{-1} anti-CEA was assembled on MoS_2-AuNPs/GCE, forming anti-CEA/MoS_2-AuNPs/GCE. Following that, 1% BSA was utilized to block possible unspecific adsorption at anti-CEA/MoS_2-AuNPs/GCE. Then, the fabricated modified electrode was incubated with target CEA for 50 min. After washing, HRP/HRP-anti-CEA/MoS_2-AuNPs nanoprobe was reacted with as-prepared CEA/BSA/anti-CEA/MoS_2-AuNPs/GCE for immunoreaction at 37 °C for 50 min, forming MoS_2-based electrochemical immunosensor.

3. Results and discussion

3.1. Proof of MoS_2-based nanoprobes

The TEM images of MoS_2 and its nanocomposite were shown in Fig. S1A and Fig. S1B, respectively, suggesting that the designed nanocomposite had been successfully synthesized. Subsequently, the whole preparation process was characterized by UV–vis spectroscopy and zeta potential analysis, proving the successful synthesis of MoS_2-AuNPs-based nanoprobes. As exhibited in Fig. 1A, with the decoration of AuNPs on MoS_2 surface, an obvious absorption peak located at 548 nm was obtained (blue curve). When HRP-anti-CEA was immobilized on MoS_2-AuNPs nanocomposite, a very weak absorption peak of HRP at 404 nm was observed (red curve). Once HRP as a blocking agent was

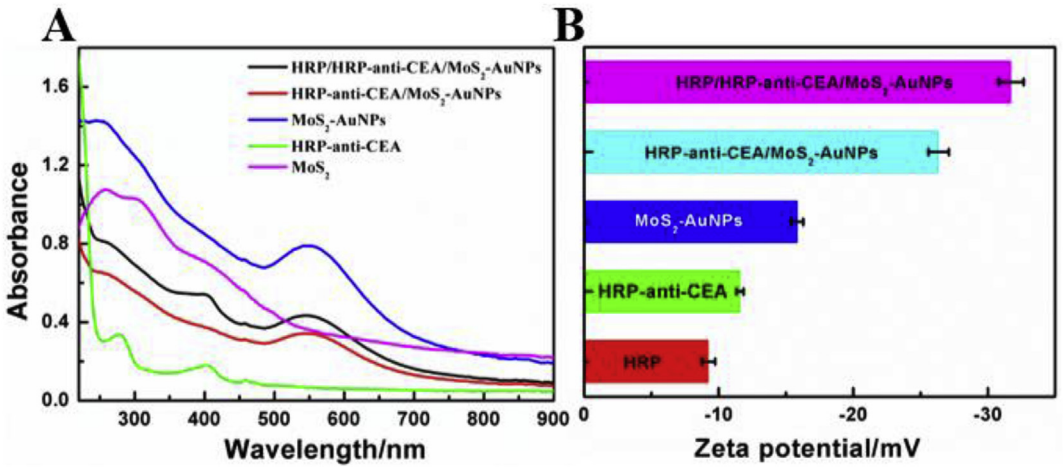

Fig. 1. (A) UV–vis spectra and (B) zeta potentials of different nanomaterials.

immobilized on HRP-anti-CEA/MoS_2-AuNPs, an obvious and typical HRP peak was obtained (black curve), further proving that HRP-anti-CEA and HRP were successfully co-immobilized on MoS_2-AuNPs nanocomposite surface. The zeta potentials of different materials also proved that our designed nanoprobes were constructed (Fig. 1B). Zeta potentials of MoS_2-AuNPs, HRP-anti-CEA/MoS_2-AuNPs and HRP/HRP-anti-CEA/MoS_2-AuNPs were −15.84 mV, −26.34 mV and −31.73 mV, respectively. Obviously, the negative HRP and HRP-anti-CEA made the potential shift negatively, further proving the amplified nanoprobes had been successfully prepared.

3.2. Fabrication of the detection strategy

Since the successful synthesis of nanoprobes, electrochemical techniques were employed to monitor the preparation of MoS_2-based detection strategy. Fig. 2A exhibited that larger redox peaks at MoS_2-AuNPs/GCE (curve b) than those at bare GCE (curve a), which was ascribed to the good conductivity of MoS_2-AuNPs. The peak currents obviously decreased at anti-CEA/MoS_2-AuNPs/GCE (curve c) and BSA/anti-CEA/MoS_2-AuNPs/GCE (curve d), respectively, suggesting nonconductive anti-CEA and BSA were assembled on modified electrode. When CEA was captured at BSA/anti-CEA/MoS_2-AuNPs/GCE, the formation of immune production made the peak current further decrease (curve e). Unexpectedly, the redox peak current suddenly increased after HRP/HRP-anti-CEA/MoS_2-AuNPs nanoprobe was incubated with the modified electrode, suggesting that the immobilized nanoprobe possessed excellent conductivity and was successfully captured by modified electrode (curve f).

We also employed EIS to confirm the prepared procedure of MoS_2-based immunosensor (Fig. 2B). If MoS_2-AuNPs nanocomposite was supported on GCE surface, a larger semicircle was obtained at MoS_2-AuNPs/GCE (curve b) compared to bare GCE (curve a). Once nonconductive anti-CEA and BSA molecules were attached to the MoS_2-AuNPs nanocomposites film, the semicircle obviously increased at anti-CEA/MoS_2-AuNPs/GCE (curve c) and BSA/anti-CEA/MoS_2-AuNPs/GCE (curve d), respectively. As expected, the semicircle further increased when BSA/anti-CEA/MoS_2-AuNPs/GCE reacted with 100 pg mL^{-1} CEA (curve e). More interestingly, the semicircle surprisingly decreased when HRP/HRP-anti-CEA/MoS_2-AuNPs nanoprobe was immobilized on modified electrode surface (curve f). The decrease was owing to the excellent conductivity of nanoprobe, which was in agreement with the CV results. Therefore, all results proved the successful preparation of MoS_2-based detection strategy for the detection of CEA.

3.3. Amplification performance of different nanoprobes

As we know, detection sensitivity was greatly depended on the properties of nanoprobes. Therefore, the catalytic activities of those nanoprobes were investigated. As shown in Fig. 3, the immunosensors were employed to analyze CEA with four kinds of signal amplification probes. In comparison, 1 ng mL^{-1} CEA was reacted with different detection strategies in the absence (curve a) and presence (curve b) of H_2O_2. It could be observed that the response current shifts ($\Delta I = I_b - I_a$) of immunosensors amplified by HRP-anti-CEA/AuNPs, BSA/HRP-anti-CEA/MoS_2-AuNPs and HRP/HRP-anti-CEA/MoS_2-AuNPs nanoprobes were 1.56, 2.60 and 4.50 times than that amplified by HRP-anti-CEA

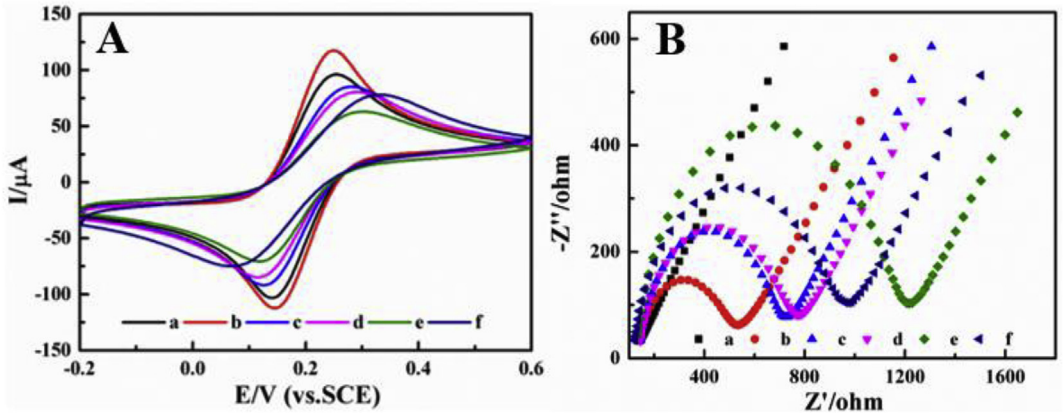

Fig. 2. (A) CV and (B) EIS curves of (a) bare GCE, (b) MoS_2-AuNPs/GCE, (c) anti-CEA/MoS_2-AuNPs/GCE, (d) BSA/anti-CEA/MoS_2-AuNPs/GCE, (e) CEA/BSA/anti-CEA/MoS_2-AuNPs/GCE and (f) nanoprobe/CEA/BSA/anti-CEA/MoS_2-AuNPs/GCE by using $[Fe(CN)_6]^{3-/4-}$ as an electrochemical indicator, respectively.

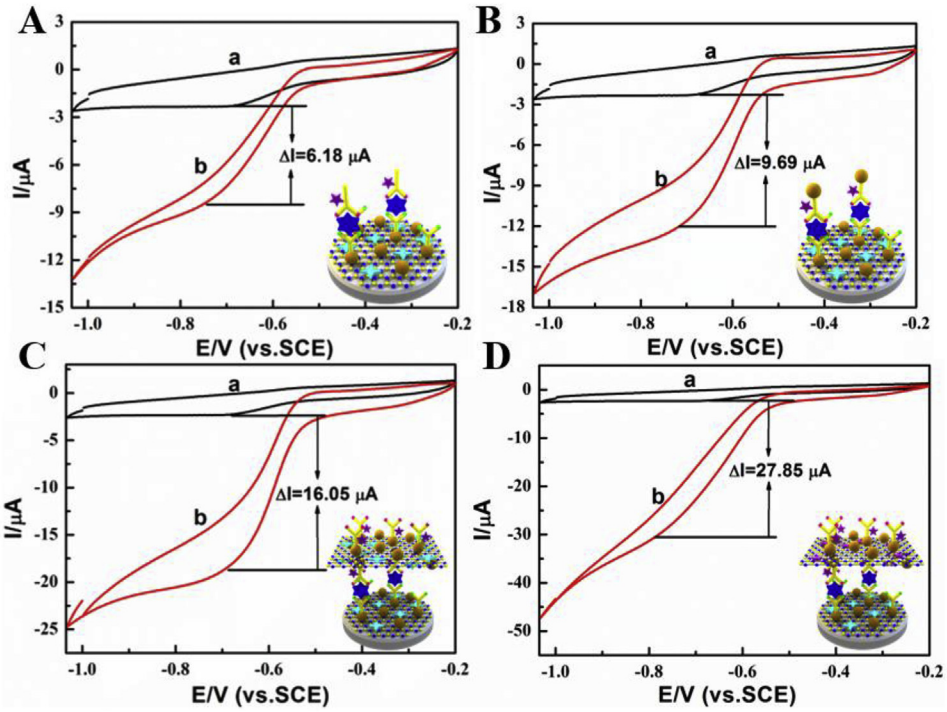

Fig. 3. CV responses of the proposed "sandwich" immunosensor formation with different probes (A) HRP-anti-CEA, (B) HRP-anti-CEA/AuNPs, (C) BSA/HRP-anti-CEA/MoS_2-AuNPs and (D) HRP/HRP-anti-CEA/MoS_2-AuNPs in 0.1 M PB in the absence (a) and presence of (b) 0.01 M o-PD + 0.16 M H_2O_2.

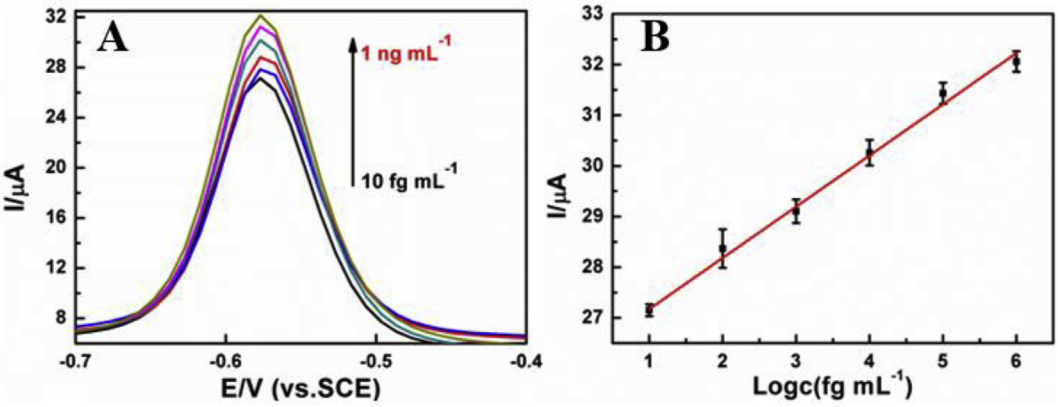

Fig. 4. (A) DPV results of MoS_2-based immunosensor for the analysis of CEA concentration (a→f): 10 fg mL^{-1}, 100 fg mL^{-1}, 1 pg mL^{-1}, 10 pg mL^{-1}, 100 pg mL^{-1} and 1 ng mL^{-1}. (B) Relationship between electrochemical responses and CEA concentration.

(6.18 μA). From this result, we could concluded that the electrochemical signal amplification was generated from the synergistically catalytic ability of HRP + AuNPs or HRP + MoS_2-AuNPs (Yang et al., 2015a). Obviously, HRP/HRP-anti-CEA/MoS_2-AuNPs nanoprobe possessed the best amplification performance among four probes. Therefore, we used HRP/HRP-anti-CEA/MoS_2-AuNPs nanoprobe to ultrasensitively detect CEA in the following experiments.

3.4. Evaluation of incubation time

To optimize the analytical performance of the MoS_2-based electrochemical immunosensor, we studied the reaction time of target CEA and HRP/HRP-anti-CEA/MoS_2-AuNPs nanoprobe. Fig. S2A exhibited that longer incubation time brought larger peak current ranging from 10 to 50 min. A maximal current response was observed at 50 min. Unfortunately, longer incubation time (over 50 min) led to the lower peak current. Thus, we chose 50 min to capture target CEA. Similarly, the optimal incubation time of nanoprobe was 50 min (Fig. S2B).

3.5. Analytical performance of the immunosensor

The analytical performance of MoS_2-based immunosensor was recorded by differential pulse voltammetry (DPV), which was generated from HRP catalyzed o-PD by H_2O_2. Fig. 4A exhibited that peak currents of MoS_2-based immunosensor increased with the detection of 10 fg mL^{-1} - 1 ng mL^{-1} CEA. According to the relationship between electrochemical responses and CEA concentration, a linear range was shown in Fig. 4B and an equation was listed as I (μA) = $0.9977\log c_{CEA}$ (fg mL^{-1}) + 26.2179 (R^2 = 0.9937). It should be noted that this as-designed detection strategy could analyze CEA concentration down to 1.2 fg mL^{-1} (S/N = 3). Table S1 summarized the analytical performance of nanoprobes-based immunosensor for CEA detection, suggesting our designed immunosensor possessed excellent detection performance.

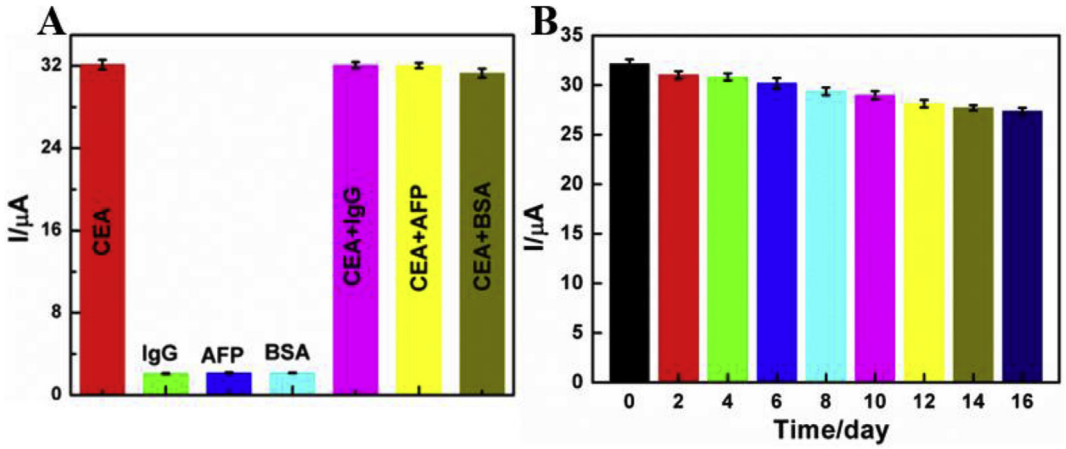

Fig. 5. Electrochemical responses of this immunosensor in the same concentration CEA, IgG, AFP, BSA solution and the mixture of CEA + lgG, CEA + AFP and CEA + BSA.

3.6. Selectivity, cross-sensitivity and stability of our detection strategy

Selectivity is an important parameter for the practical application of this as-prepared immunosensor. In this work, α-fetoprotein antigen (AFP), bovine serum albumin (BSA) and human immunoglobulin G (IgG) were selected as interfering species, respectively. Fig. 5A showed the DPV signals of IgG, AFP and BSA were about 2.1%, 3.1% and 2.6% of peak current of CEA at the same concentration (1 ng mL^{-1}). Moreover, the presence of IgG, AFP and BSA did not interfere with CEA detection of the immunosensor, suggesting that the MoS_2-based immunosensor possessed excellent selectivity.

Furthermore, the long-term stability was tested. About 14.8% electrochemical signal decreased compared with its initial value after 16 days storage, indicating the designed immunosensor had good stability (Fig. 5B).

3.7. Practical application

According to the above results, the application of this MoS_2-based immunosensor for real samples was studied. From Table S2, high recovery (> 98%) and small relative standard deviation (RSD, < 10%) were obtained, respectively, indicating that the designed immunosensor could analyze CEA in simulated samples with accepted results.

4. Conclusion

We constructed an ultrasensitive MoS_2-based electrochemical sensing strategy for the CEA analysis combined with enzyme-assisted signal amplification strategy. MoS_2-AuNPs nanocomposites were not only used as electrode modified materials, but also employed to prepare nanoprobes due to their enzyme mimics and excellent conductivity. Due to the triple signal amplification effect, this designed detection strategy exhibited ultrahigh sensitivity, low detection limit (1.2 fg mL^{-1}), high selectivity and stability. More importantly, this as-prepared immunosensor could determine CEA in serum samples, indicating that MoS_2-based nanohybrids was a powerful nanomaterial to construct biosensors for clinical analysis.

Declaration of interests

None.

CRediT authorship contribution statement

Shao Su: Conceptualization, Writing - review & editing. **Qian Sun:** Methodology, Investigation. **Ling Wan:** Methodology, Data curation. **Xiaodan Gu:** Investigation, Formal analysis. **Dan Zhu:** Formal analysis, Writing - original draft. **Yi Zhou:** Resources, Visualization. **Jie Chao:** Writing - review & editing, Supervision. **Lianhui Wang:** Project administration, Funding acquisition.

Acknowledgements

This work was supported by the National Key Research and Development Program of China (2017YFA0205302), the National Natural Science Foundation of China (61671250 and 21475064), the Program for Changjiang Scholars and Innovative Research Team in University (IRT_15R37), the Key Research and Development Program of Jiangsu (BE2018732), the Natural Science Key Fund for Colleges, Universities in Jiangsu Province (17KJA430011), the Scientific Research Foundation of Nanjing University of Posts and Telecommunications (NY218032) and CAS Key Laboratory of Interfacial Physics and Technology (CASKL-IPT1701).

Appendix A. Supplementary data

Supplementary data to this article can be found online at https://doi.org/10.1016/j.bios.2019.111353.

References

Chen, P., Pan, D., Fan, C.H., Chen, J.H., Huang, K., Wang, D.F., Zhang, H.L., Li, Y., Feng, G.Y., Liang, P.J., 2011. Nat. Nanotechnol. 6, 639–644.
Devi, R., Gogoi, S., Barua, S., Dutta, H.S., Bordoloi, M., Khan, R., 2019. Food Chem. 276, 350–357.
Du, D., Zou, Z., Shin, Y., Wang, J., Wu, H., Engelhard, M.H., Liu, J., Aksay, I.A., Lin, Y., 2010. Anal. Chem. 82, 2989–2995.
Fan, C.H., Yi, Z., Li, G., Zhu, J., Zhu, D., 2000. Electroanalysis 12, 1156–1158.
Farka, Z., Juřík, T., Kovář, D., Trnková, L., Skládal, P., 2017. Chem. Rev. 117, 9973–10042.
Feng, T., Qiao, X., Wang, H., Sun, Z., Hong, C., 2016. Biosens. Bioelectron. 79, 48–54.
Ge, Z.L., Pei, H., Wang, L.H., Song, S.P., Fan, C.H., 2011. Sci. China Chem. 54, 1273–1276.
He, S., Song, B., Li, D., Zhu, C., Qi, W., Wen, Y., Wang, L., Song, S., Fang, H., Fan, C.H., 2010. Adv. Funct. Mater. 20, 453–459.
Huang, Y., Gao, L., Cui, H., 2018. ACS Appl. Mater. Interfaces 10, 17040–17046.
Jiang, D., Du, X., Liu, Q., Zhou, L., Qian, J., Wang, K., 2015. ACS Appl. Mater. Interfaces 7, 3093–3100.
Kong, F.Y., Xu, Z., Xu, M.T., Xu, J.J., Chen, H.Y., 2011. Electrochim. Acta 56, 9386–9390.
Li, J., Song, S., Liu, X., Wang, L., Pan, D., Huang, Q., Zhao, Y., Fan, C.H., 2008. *Adv. Mater.* 20, 497–500.
Li, N., Wang, Y., Cao, W., Zhang, Y., Yan, T., Du, B., Wei, Q., 2015. J. Mater. Chem. B 3, 2006–2011.
Li, Y., Zhu, W., Kang, Q., Yang, L., Zhang, Y., Wang, Y., Wei, Q., 2018. ACS Appl. Mater. Interfaces 10, 38791–38798.
Lin, D., Wu, J., Wang, M., Yan, F., Ju, H., 2012. Anal. Chem. 84, 3662–3668.
Lin, M.H., Wang, J.J., Zhou, G.B., Wang, J.B., Wu, N., Lu, J.X., Gao, J.M., Chen, X.Q., Shi, J.Y., Zuo, X.L., Fan, C.H., 2015. Angew. Chem. Int. Ed. 127, 2179–2183.

Liu, H., Wu, X., Zhang, X., Burda, C., Zhu, J.J., 2012. J. Phys. Chem. C 116, 2548–2554.
Lu, J., Liu, S., Ge, S., Yan, M., Yu, J., Hu, X., 2012. Biosens. Bioelectron. 33, 29–35.
Miao, X., Cheng, Z., Ma, H., Li, Z., Xue, N., Wang, P., 2017. Anal. Chem. 90, 1098–1103.
Pang, P.F., Teng, X., Chen, M., Zhang, Y.L., Wang, H.B., Yang, C., Yang, W.R., Barrow, C.J., 2018. Sensor. Actuator. B Chem. 266, 400–407.
Pei, H., Li, J., Yao, G.B., Li, J., Huang, Q., Fan, C.H., 2012. Angew. Chem. Int. Ed. 51 9185-9185.
Peng, G., Li, X.Y., Cui, F., Qiu, Q.Y., Chen, X.J., Huang, H., 2018. ACS Appl. Mater. Interfaces 10, 17551–17559.
Ren, X., Ma, H., Zhang, T., Zhang, Y., Yan, T., Du, B., Wei, Q., 2017. ACS Appl. Mater. Interfaces 9, 37637–37644.
Shen, W.J., Zhuo, Y., Chai, Y.Q., Yang, Z.H., Han, J., Yuan, R., 2015. ACS Appl. Mater. Interfaces 7, 4127–4134.
Su, S., Zhang, C., Yuwen, L.H., Chao, J., Zuo, X.L., Liu, X., Song, C.Y., Fan, C.H., Wang, L.H., 2014. ACS Appl. Mater. Interfaces 6, 18735–18741.
Su, S., Zou, M., Zhao, H., Yuan, C.F., Xu, Y.N., Zhang, C., Wang, L.H., Fan, C.H., Wang, L.H., 2015. Nanoscale 7, 19129–19135.
Su, S., Sun, H.F., Cao, W.F., Chao, J., Peng, H., Zuo, X., Yuwen, L.H., Fan, C.H., Wang, L.H., 2016. ACS Appl. Mater. Interfaces 8, 6826–6833.
Su, S., Cao, W.F., Liu, W., Lu, Z.W., Zhu, D., Chao, J., Weng, L.X., Wang, L.H., Fan, C.H., Wang, L.H., 2017. Biosens. Bioelectron. 94, 552–559.
Su, S., Li, J., Yao, Y., Sun, Q., Zhao, Q., Wang, F., Li, Q., Liu, X., Wang, L., 2019. ACS Appl. Bio Mater. 2, 292–298.
Sun, G., Lu, J., Ge, S., Song, X., Yu, J., Yan, M., Huang, J., 2013. Anal. Chim. Acta 775, 85–92.
Sun, H.F., Chao, J., Zuo, X.L., Su, S., Liu, X., Yuwen, L.H., Fan, C.H., Wang, L.H., 2014. RSC Adv. 4, 27625.
Tang, D.P., Yuan, R., Chai, Y.Q., 2008. Anal. Chem. 80, 1582–1588.
Wan, Y., Deng, W., Su, Y., Zhu, X., Peng, C., Hu, H., Peng, H., Song, S., Fan, C.H., 2011. Biosens. Bioelectron. 30, 93–99.
Wan, Y., Su, Y., Zhu, X., Liu, G., Fan, C.H., 2013. Biosens. Bioelectron. 47, 1–11.
Wang, Z., Liu, N., Ma, Z., 2014. Biosens. Bioelectron. 53, 324–329.
Wang, S., Yang, F., Jin, D., Dai, Q., Tu, J., Liu, Y., Ning, Y., Zhang, G.J., 2017. Anal. Chem. 89, 5349–5356.
Wen, Y., Pei, H., Shen, Y., Xi, J., Lin, M.H., Lu, N., Shen, X., Li, J., Fan, C.H., 2013. Sci. Rep. 3, 867.
Wu, D., Ma, H., Zhang, Y., Jia, H., Yan, T., Wei, Q., 2015. ACS Appl. Mater. Interfaces 7, 18786–18793.
Xiu, W., Chu, C., Lei, S., Deng, W., Mei, Y., Ge, S., Yu, J., Song, X., 2015. Sensor. Actuator. B Chem. 206, 30–36.
Yan, J., Mei, H., Di, L., Yao, H., Rui, Z., Jiang, X., Song, S., Wang, L., Fan, C.H., 2008. Nano Res. 1, 490–496.
Yang, Y.C., Dong, S.W., Shen, T., Jian, C.X., Chang, H.J., Li, Y., Zhou, J.X., 2011. Electrochim. Acta 56, 6021–6025.
Yang, F., Yang, Z., Zhuo, Y., Chai, Y., Yuan, R., 2015a. Biosens. Bioelectron. 66, 356–362.
Yang, Z.H., Zhuo, Y., Yuan, R., Chai, Y.Q., 2015b. Biosens. Bioelectron. 69, 321–327.
Yang, Z.H., Zhuo, Y., Yuan, R., Chai, Y.Q., 2016. Biosens. Bioelectron. 78, 321–327.
Yang, H.Y., Wang, H.J., Xiong, C.Y., Chai, Y.Q., Yuan, R., 2017. ACS Appl. Mater. Interfaces 9, 36239–36246.
Yuan, L., Xu, L., Liu, S., 2012. Anal. Chem. 84, 10737–10744.
Zhao, Y., Liu, L., Kong, D., Kuang, H., Wang, L., Xu, C., 2014. ACS Appl. Mater. Interfaces 6, 21178–21183.
Zhong, Z., Wu, W., Wang, D., Wang, D., Shan, J., Yi, Q., Zhang, Z., 2010. Biosens. Bioelectron. 25, 2379–2383.
Zhou, J., Lai, W., Zhuang, J., Tang, J., Tang, D., 2013. ACS Appl. Mater. Interfaces 5, 2773–2781.
Zhou, L., Huang, J., Yu, B., Liu, Y., You, T., 2015. ACS Appl. Mater. Interfaces 7, 24438–24445.
Zuo, X., Cheng, P., Huang, Q., Song, S., Wang, L., Di, L., Fan, C.H., 2009. Nano Res. 2, 617–623.